Int J Adv Manuf Technol (2013) 67:1833–1845
DOI 10.1007/s00170-012-4612-3

ORIGINAL ARTICLE

Cutting force prediction for ball-end mills with non-horizontal and rotational cutting motions

Abdullahil Azeem · Hsi-Yung Feng

Received: 15 November 2011 / Accepted: 30 October 2012 / Published online: 14 November 2012

Abstract Accurate cutting force prediction is essential to precision machining operations as cutting force is a process variable that directly relates to machining quality and efficiency. This paper presents an improved mechanistic cutting force model for multi-axis ball-end milling. Multi-axis ball-end milling is mainly used for sculptured surface machining where non-horizontal (upward and downward) and rotational cutting tool motions are common. Unlike the existing research studies, the present work attempts to explicitly consider the effect of the 3D cutting motions of the ball-end mill on the cutting forces. The main feature of the present work is thus the proposed generalized concept of characterizing the undeformed chip thickness for 3D cutter movements. The proposed concept evaluates the undeformed chip thickness of an engaged cutting element in the principal normal direction of its 3D trochoidal trajectory. This concept is unique and it leads to the first cutting force model that specifically applies to non-horizontal and rotational cutting tool motions. The resulting cutting force model has been validated experimentally with extensive verification test cuts consisting of horizontal, non-horizontal, and rotational cutting motions of a ball-end mill.

Keywords Cutting force · Ball-end milling · Non-horizontal cutting motion · Rotational cutting motion · Undeformed chip thickness

A. Azeem (✉)
Department of Industrial and Production Engineering,
Bangladesh University of Engineering and Technology,
Dhaka 1000, Bangladesh
e-mail: azeem@ipe.buet.ac.bd

H.-Y. Feng
Department of Mechanical Engineering,
The University of British Columbia,
Vancouver, BC, Canada V6T 1Z4

1 Introduction

Mechanical parts with complex sculptured surfaces are widely employed and produced in practice such as dies and molds in the automotive industry and compressor and turbine blades in the aerospace industry. The ball-end milling process is one of the most common machining processes to produce these complex surfaces. Product quality and productivity are two primary concerns in manufacturing. It is important to select optimal cutting parameters according to a physics-based method in order to ensure machined surface quality and to reduce or even eliminate the inefficiency involved in the traditional trial-and-error practice. Cutting forces acting on a ball-end mill is a significant physical variable as they encapsulate critical cutting information. Reliable prediction of cutting forces is thus crucial in selecting the optimal cutting parameters that would result in high efficiency and maintain the required part quality.

Accurate cutting force predictions from a cutting force model for a given machining process depend on the reliability of the model input and derived parameters. The undeformed chip thickness is one such parameter. A detailed analysis of the undeformed chip geometry along a cutting edge was first provided by Martellotti [1]. He showed that the true trajectory of a milling tooth is a trochoidal curve; however, if the cutting speed is much larger than the feed rate, a circular trajectory can be used as a valid approximation. With this approximation, the undeformed chip thickness has been formulated with ease and expressed by many researchers as the radial distance between two consecutive circular tooth trajectories. For mechanistic cutting force modeling, this concept of undeformed chip thickness was first adopted for end milling by Kline et al. [2]. This pioneering work was later extended to incorporate cutter runout and cutting system flexibility in the determination of chip thickness [3, 4]. To further improve cutting force prediction accuracy, continued studies on the undeformed chip thickness determination in milling have been carried

out by employing the true trochoidal cutting trajectory in horizontal linear tool motions [5, 6] as well as in horizontal circular tool motions [7]. In the context of reliable calibration of the associated empirical cutting force coefficients, other proven concepts for characterizing the undeformed chip thickness were introduced, including the average chip–tool contact length on the rake faces of a cutting edge [8] and derivations using experimentally established orthogonal cutting databases [9].

The studies referenced earlier all focused on flat-end milling tools moving on a horizontal plane. The geometry of a ball-end mill is notably complex compared with that of a flat-end mill. Cutting edges on the cylindrical part of a ball-end mill are deemed geometrically the same as those of a flat-end mill, whereas on the ball part they change continuously along the cutter axis. This leads to discrepancies, in particular, in the direction of defining and determining the undeformed chip thicknesses for the ball-end mill cutting elements. Yang and Park [10] were the first to introduce a cutting force model for ball-end milling. The undeformed chip thickness was determined in the cutter surface normal direction. This direction was later adopted by several other researchers [11–15]. In contrast, Feng and Menq [16] formulated their mechanistic cutting force model for ball-end milling by defining the undeformed chip thickness as the radial distance between two consecutive cutting edge trajectories in the horizontal direction. This horizontal undeformed chip thickness determination direction was also employed in various studies on ball-end milling force modeling [17–19].

It should be emphasized here again that the primary application of ball-end milling is in the finish machining of sculptured surfaces. Sculptured surface machining is geometrically very complex and involves many process variables [20]. A reliable cutting force model is essential to the associated process planning tasks such as determining the milling tool path that minimizes tool deflections [21]. Notwithstanding the good number of published papers on ball-end milling force modeling, the complexity attributed to the sculptured surface geometry has not been well examined. Specifically, studies that modeled the ball-end milling forces for inclined (or non-horizontal) feed motions [22] or with explicit consideration of the sculptured surface curvature [23] were reported only recently. It is believed that the present work introduces the first ball-end milling force model that applies to multi-axis non-horizontal and rotational cutting tool motions.

2 Undeformed chip thickness determination direction

The two existing directions to determine the undeformed chip thickness for horizontal ball-end milling are illustrated in Fig. 1. A geometric relationship can be easily observed between the undeformed chip thickness and chip width for these two concepts through the undeformed chip area, the product of the chip width with the chip thickness. For the surface normal direction concept, the undeformed chip area is b_1t_1, whereas for the horizontal direction concept it is b_2t_2. The chip width b_1 and thickness t_1 can be shown, for a small cutting edge element at an angular position γ with respect to the cutter axis, to be related to b_2 and t_2 as:

$$b_1 = b_2/\sin\gamma \quad t_1 = t_2\sin\gamma \tag{1}$$

It is then clear that the undeformed chip area for the surface normal direction concept is equivalent to that for the horizontal direction concept:

$$b_1t_1 = (b_2/\sin\gamma)(t_2\sin\gamma) = b_2t_2 \tag{2}$$

This indicates that, for the undeformed chip area, there is no quantitative difference between the surface normal and the horizontal direction concept. The chip area has sometimes been used as an individual term in formulating the cutting forces when the size effect in metal cutting mechanics is not explicitly considered. However, the size effect does exist and is a very important factor in modeling cutting forces under varying cutting conditions and should not be ignored [24]. As a result, many existing cutting force models elected to specifically formulate the undeformed chip thickness (instead of the chip area) in order to yield reliable cutting force predictions.

The two undeformed chip thickness determination directions discussed above were originally defined for horizontal cutting motions of the ball-end mill. Horizontal ball-end milling only has very limited applications as ball-end mills are often used in three- or multi-axis sculptured surface machining, where non-horizontal and/or rotational cutting motions are common. For non-horizontal ball-end milling

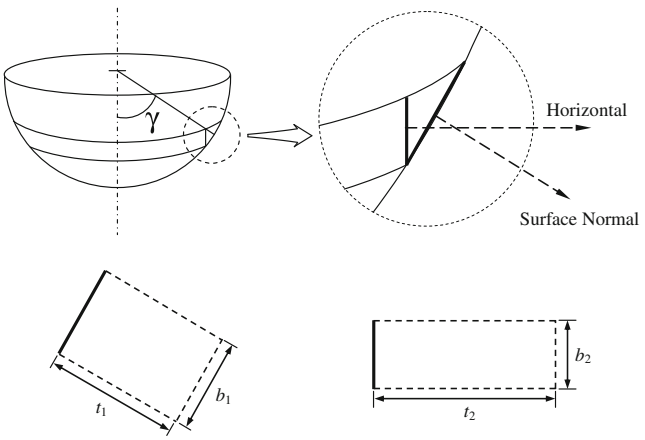

Fig. 1 Existing undeformed chip thickness determination directions for horizontal ball-end milling

cuts, researchers have consistently applied one of the two existing directions: cutter surface normal direction [25–28] and horizontal direction [29–31]. Nonetheless, these two directions, as originally proposed for horizontal cuts, may not characterize non-horizontal and rotational cuts correctly. Notably, Kim et al. [32] introduced a different concept and proposed to use the cutter feed direction to determine the undeformed chip thickness for non-horizontal cuts. As for the much more complex rotational ball-end milling cuts (due to the continuously changing cutter feed direction), only the cutter surface normal direction has been applied to the determination of the undeformed chip thickness [33, 34].

In this work, instead of considering the undeformed chip thickness individually for horizontal, non-horizontal, and rotational cutting motions, a generalized concept to determine the undeformed chip thickness is proposed to address all these basic cutting motions in multi-axis ball-end milling as a whole. Unlike the existing concepts, this newly proposed concept determines the undeformed chip thickness of a cutting edge element based on its individual cutting trajectory rather than the bulk movement of the cutter. Relevant details are to be provided in the next two sections.

3 Cutting element trajectory

The trajectory of a cutting edge element generated by a milling cutter was first mathematically derived by Martellotti [1]. For a given milling operation, the trajectory can be produced by an imaginary setup as shown in Fig. 2 where the cutter rotates in the clockwise direction. The milling cutter moves along the X axis as the imaginary pinion rolls on the imaginary rack. Curve segments AN and AN′ represent the typical trajectories generated by two consecutive cutting edge elements. These two trajectories establish the associated undeformed chip section. The

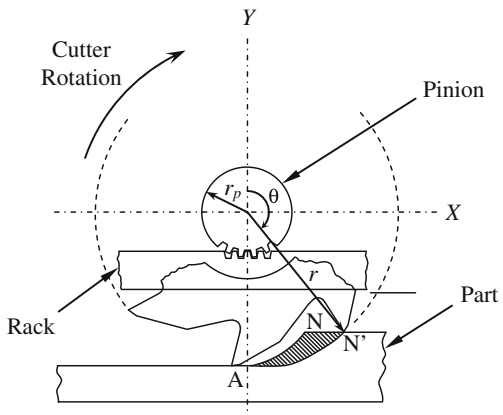

Fig. 2 Cutting element trajectory generation in peripheral milling

mathematical expression of the generated trajectory can be expressed as:

$$X = r\sin\theta \pm r_p\theta \tag{3a}$$

$$Y = r\cos\theta \tag{3b}$$

where r denotes the cutting radius, θ the angular position of the cutting element with respect to the $+Y$ direction, and r_p the imaginary pinion radius. The plus and minus signs in Eq. (3a) correspond to the two types of peripheral milling: up milling (feeding in the $+X$ direction) and down milling (feeding in the $-X$ direction), respectively. The pinion radius r_p can be expressed in terms of f (feed per tooth) and n (number of cutting edges of the cutter) as:

$$r_p = \frac{fn}{2\pi} \tag{4}$$

For a given ball-end mill, a generalized mathematical expression for the trajectory of the cutting element at a point **P** on the ith cutting edge at a distance z along the cutter axis (which is the z axis of the local cutter coordinate system) from the cutter tip (the z axis origin) can be formulated as:

$$\mathbf{P}(i,z,\theta,\boldsymbol{f},\alpha) = \begin{bmatrix} X \\ Y \\ Z \end{bmatrix} = F_3(\alpha)F_1(i,z,\theta) + F_2(f) \tag{5}$$

where f is the linear feed (in mm/tooth) and α is the rotational feed (in rad/tooth). The function F_1 specifies the cutter rotation about its axis which applies to all types of cutting motion. F_2 and F_3 are, respectively, the linear and rotational feed functions of the cutter movement. Based on Eq. (5), the mathematical expressions for the cutting element trajectories for horizontal, non-horizontal, and rotational cutting motions are readily obtainable and summarized in the following subsections.

3.1 Horizontal cutting motion

For horizontal cutting motions, the three functions in the generalized cutting element trajectory expression of Eq. (5) for a cutting element at z_0 can be written as:

$$F_1 = \begin{bmatrix} r_i(z_0)\sin\theta \\ r_i(z_0)\cos\theta \\ z_0 \end{bmatrix} \quad F_2 = \begin{bmatrix} f_l\theta \\ 0 \\ 0 \end{bmatrix} \quad F_3 = \mathbf{I} \tag{6}$$

where $r_i(z)$ is the actual cutting radius (considering cutter runout) of a cutting element at z from the ball-end mill tip. Equivalent to r_p formulated in Eq. (4), f_l is the linear feed per angular rotation unit of the cutter. Since no rotational movement of the cutter is involved, F_3 is simply a unit matrix.

3.2 Non-horizontal cutting motion

For non-horizontal cutting motions, the linear feed f_l is first decomposed into two components (a horizontal and a vertical component), which are subsequently incorporated into the linear feed function F_2. The three functions in Eq. (5) for a cutting element at z_0 can then be expressed as:

$$F_1 = \begin{bmatrix} r_i(z_0)\sin\theta \\ r_i(z_0)\cos\theta \\ z_0 \end{bmatrix} \quad F_2 = \begin{bmatrix} (f_l\cos\psi)\theta \\ 0 \\ (f_l\sin\psi)\theta \end{bmatrix} \quad F_3 = \mathbf{I} \tag{7}$$

where ψ is the non-horizontal feed angle of the ball-end mill. Like the horizontal cutting motions, F_3 is also a unit matrix as no rotational cutter movement is involved.

3.3 Rotational cutting motion

For rotational cutting motions, both the linear and rotational feed functions F_2 and F_3 are different from those for the horizontal and non-horizontal cutting motions. As no linear cutter movement is involved, F_2=0, whereas F_3 is no longer a unit matrix. The three functions in Eq. (5) for a cutting element at z_0 can now be expressed as:

$$F_1 = \begin{bmatrix} r_i(z_0)\sin\theta \\ r_i(z_0)\cos\theta \\ R+z_0 \end{bmatrix} \quad F_2 = 0 \quad F_3 = \begin{bmatrix} \cos(f_r\theta) & 0 & \sin(f_r\theta) \\ 0 & 1 & 0 \\ -\sin(f_r\theta) & 0 & \cos(f_r\theta) \end{bmatrix} \tag{8}$$

where R is the rotational radius of the cutter tip with respect to the rotational axis of the machine table (for a table-rotating machine tool) and f_r is the rotational feed per angular rotation unit of the cutter, which is $\alpha n/2\pi$. Typical cutting element trajectories for the rotational as well as horizontal and non-horizontal cutting motions are depicted in Fig. 3.

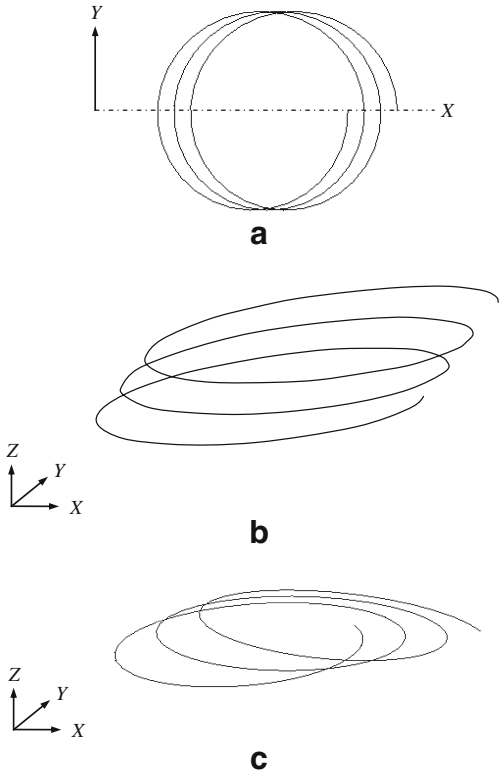

Fig. 3 Cutting element trajectories: **a** horizontal, **b** non-horizontal, and **c** rotational cutting motions

4 Undeformed chip thickness determination

In this work, the undeformed chip thickness for a cutting element is determined according to its cutting trajectory. A generalized 3D evaluation procedure is proposed, which is applicable to all cutting motions in multi-axis ball-end milling. Suppose a cutting element P is moving along its cutting trajectory $T_P(X, Y, Z)$. The undeformed chip thickness for P at any instant is determined along the principal normal direction of T_P at P. The principal normal direction is directed towards the center of the osculating circle of T_P at P, which is the circle in the osculating plane at P that best approximates T_P (just like the tangent of T_P at P is the line that best approximates T_P at P). More specifically, the center of the osculating circle $\mathbf{P}_0$ is regarded as the instantaneous revolving center of P as it moves along T_P. $\mathbf{P}_0$ can be expressed as:

$$\mathbf{P}_0 = P + \frac{1}{\kappa_P}\mathbf{N_P} \tag{9}$$

where κ_P is the curvature of T_P at P and $\mathbf{N_P}$ is the unit vector of the principal normal direction.

As the undeformed chip thickness for P is to be determined along $\mathbf{N_P}$ or $\overline{PP_0}$ (the line connecting the cutting element P and its instantaneous revolving center $\mathbf{P}_0$), it is necessary to identify the intersection points of $\overline{PP_0}$ with the machined surfaces generated by all the cutting edges in the previous cutter rotation cycle (Fig. 4). Identification of all the intersection points is needed in order to determine all the undeformed chip thickness candidates [3, 4, 29, 35]. The smallest-value candidate is the undeformed chip thickness solution, which is taken as zero if negative. Calculating the intersection points is quite complex for non-horizontal and rotational cutting motions of a ball-end mill compared to that for horizontal cutting motions. Relevant details are given in the following subsections.

4.1 Horizontal cutting motion

For horizontal cutting motions, the trajectories of all the involved cutting elements are on the same horizontal (XY)

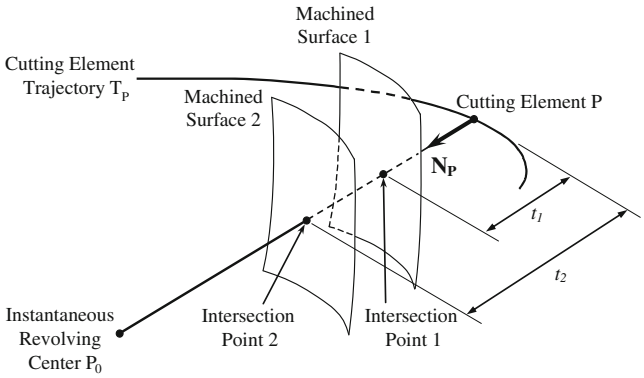

Fig. 4 Geometry to determine the undeformed chip thickness

plane (Fig. 3a). It is thus evident that the intersection points of $\overline{PP_0}$ with the previously generated surfaces are on the same plane as well. In other words, P, $\mathbf{P}_0$, and the intersection points will have the same Z value. Hence, only the trajectory expressions for the corresponding cutting elements (of the same z_0 height on the cutter) are required to solve for the intersection points. From the mathematical expressions of Eqs. (5) and (6), the only unknown variable to be solved is the angular position θ of each corresponding cutting element along its respective cutting trajectory for the corresponding intersection point.

4.2 Non-horizontal cutting motion

Unlike horizontal cutting motions, the cutting element trajectories for non-horizontal cutting motions of a ball-end mill are not on the same plane (Fig. 3b). For a cutting element P along its trajectory, its instantaneous revolving center $\mathbf{P}_0$ now lies on a different Z plane. As a result, the intersection points of $\overline{PP_0}$ with the previously generated surfaces will also be on different Z planes. Also, the intersection points can no longer be found on the trajectories of cutting elements at the same z_0 height on the cutter. This makes the solving for the intersection points more complicated than that for the horizontal cutting motions as both the cutting element position z and θ need to be solved for each cutting edge in the previous cutter rotation cycle using Eqs. (5) and (7).

The solution is obtained numerically via a two-step iterative process. The cutting element position z is first computed based on the assumption of the same angular position θ. The angular position θ for the intersection point is then updated with the computed cutting element position z. The solving process then goes back to update the cutting element position z. This iterative process continues until the computed values of both the cutting element position z and θ stabilize numerically.

4.3 Rotational cutting motion

Like non-horizontal cutting motions, the cutting element trajectories for rotational cutting motions of a ball-end mill do not lie on the same plane (Fig. 3c). Since a cutting element P and its instantaneous revolving center $\mathbf{P}_0$ are on different Z planes for rotational cutting motions, the same two-step iterative process employed for non-horizontal cutting motions is also applicable here to solve for the two unknown variables z and θ from the cutting trajectory expressions of Eqs. (5) and (8). Nonetheless, the rotational movement of the machine table coupled with the spindle/cutter rotation results in a very complex and highly nonlinear problem to solve for the two variables. Common nonlinear solvers such as the Newton–Raphson method to compute the cutting element position z often yields a local solution instead of the desired global solution. This much affects the accuracy of the undeformed chip thickness to be determined.

To ensure solution accuracy, a solving process based on incremental marching search has been devised for the two unknown variables. By incrementally varying the values of z and θ, a good number of point positions can be obtained via Eqs. (5) and (8). Based on the fact that the intersection points on the previously generated surfaces would lie in between P and $\mathbf{P}_0$, the search domain for z is set according to the z coordinates of these two points. Moreover, as all the involved cutting element trajectories are very close to the cutting trajectory of P (due to the large cutting speed to feed rate ratio), the search domain for θ is set according to the position of P along its trajectory. Of all the searched positions on a previously generated surface, the closest position to $\overline{PP_0}$ is taken as the intersection point.

4.4 Undeformed chip thickness and width

For a given cutting motion, the intersection point on each generated surface in the previous cutter rotation cycle is readily identified using the procedure presented in "Sections 4.1–4.3". The distance from the cutting element to each intersection point represents an undeformed chip thickness candidate. For a ball-end mill with n cutting edges, n undeformed chip thickness candidates are obtained from the n intersection points (for example, t_1 and t_2 in Fig. 4 for a two-flute ball-end mill). As stated previously, the candidate with the smallest value is the solution for the undeformed chip thickness. The undeformed chip thickness is taken as zero if the smallest value is negative. This indicates that the cutting element is in fact not removing any material at this instant, often due to the effect of cutter runout. It should be noted, however, that for cutting elements close to the cutter tip in downward and rotational cutting motions, there will

not be any machined surfaces generated by the cutting edges in the previous cutter rotation cycle for $\overline{PP_0}$ to intersect. In this case, the segment length of $\overline{PP_0}$ is taken as the undeformed chip thickness for the cutting element P.

Once the undeformed chip thickness is determined for a cutting element, the undeformed chip width needs to be quantified as well in order to reliably calculate the cutting forces acting on the cutting element. The undeformed chip width is defined perpendicular to the undeformed chip thickness. The reason is simply that the undeformed chip area (which directly contributes to the material removal rate) is the product of undeformed chip thickness and width. For horizontal cutting motions, as the undeformed chip thickness is defined horizontally, the size (thickness) of the cutting element (disk) is the undeformed chip width. However, for non-horizontal and rotational cutting motions, the chip thickness is not defined horizontally anymore; hence, the cutting element size (cutting disk thickness) cannot be used as the undeformed chip width directly. The direction to determine the undeformed chip thickness instead needs to be applied and incorporated in the calculation of the undeformed chip width.

4.5 Results and comparison

The undeformed chip thickness values for each of the three basic cutting motions in multi-axis ball-end milling using the proposed concept were calculated and compared with those using the existing concepts. For horizontal cutting motions, results from the proposed and existing concepts were the same, as expected. However, for non-horizontal and rotational cutting motions, the undeformed chip thickness values from the proposed and existing concepts were found to differ quite significantly.

Figure 5 illustrates a typical comparison of the undeformed chip thickness values determined using the proposed concept against those using the existing concepts (based on the horizontal or feed direction) for upward and downward cutting motions. It can be seen that, due to the non-planar cutting trajectories, the existing concepts over-estimate the undeformed chip thicknesses for upward cutting motions and under-estimate them for downward cutting motions, in particular for cutting elements close to the cutter tip.

Feng and Menq [16, 29] attempted to determine the undeformed chip thickness for non-horizontal cutting motions of a ball-end mill by formulating and adding the specific contribution of the vertical feed component of the cutter to the undeformed chip thickness. This results in the same undeformed chip thickness values as those obtained using the proposed concept. Unfortunately, this existing concept is not applicable to determining the undeformed chip thickness for rotational cutting motions

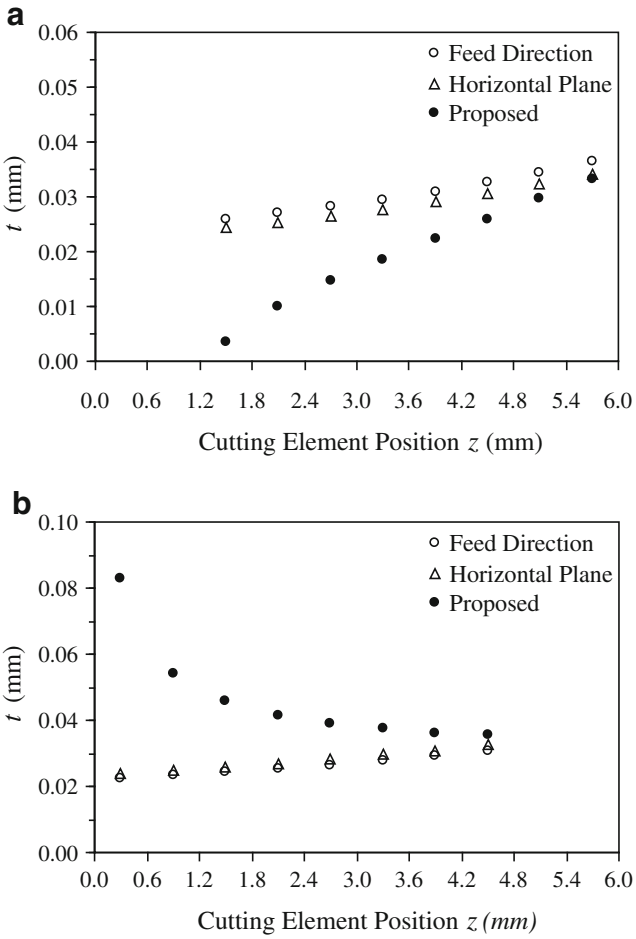

Fig. 5 Undeformed chip thickness values at θ=60°: **a** 20° upward and **b** 20° downward cutting motion (feed 0.043 mm/tooth, axial depth of cut 6 mm, side step 6 mm)

because rotational feed acts much differently than linear feed. It is thus necessary to develop a generic concept that could be applied to determining the undeformed chip thickness for all the three basic cutting motions in multi-axis ball-end milling.

In rotational cutting motions, angular displacements of all the cutting edge elements on a ball-end mill are the same. However, the resulting linear displacements differ due to the varying distance of each cutting element to the rotating center of the machine table (for table-rotating machine tools). This distance increases as the cutting element moves away from the cutter tip. The varying linear displacements for cutting elements along the cutter axis clearly much affect the undeformed chip thickness calculation in rotational cutting motions.

The calculated undeformed chip thickness values using the proposed concept are compared against those using the approximated horizontal concept (Fig. 6). By equating the instantaneous linear feed rate at the cutter tip, the approximated horizontal concept approximates the 3D rotational

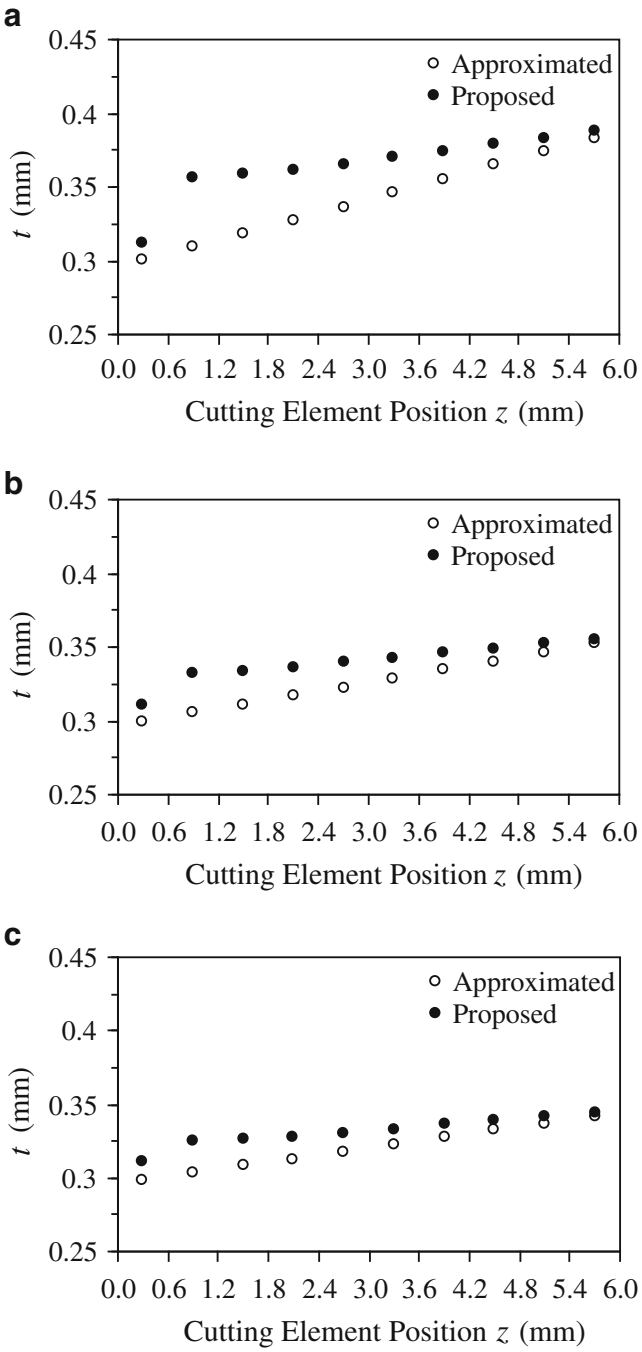

Fig. 6 Undeformed chip thickness values at θ=60° for rotational cutting motions: **a** R=30 mm, **b** R=60 mm, and **c** R=90 mm (feed at cutter tip 0.337 mm/tooth, axial depth of cut 6 mm, side step 6 mm)

cutting motion as a 2D horizontal cutting motion with linearly varying feed along the cutter axis. In Fig. 6, it can be seen that the difference of undeformed chip thickness values calculated using the proposed and the approximated concept is in fact quite significant and, as expected, increases with decreasing rotating arm length of the cutter tip. A comparison of undeformed chip thickness values was also made between the rotational and the regular horizontal cutting motion with the same instantaneous linear feed rate at the cutter tip (Fig. 7). It is shown that with decreasing rotating arm length of the cutter tip, undeformed chip thickness values for the rotational cutting motion move away from those for the horizontal motion as expected.

5 Calibration of cutting force coefficients

The empirical chip–force relationship employed in the present work is formulated as follows [35]:

$$\mathrm{d}\,F_{\mathrm{T}}(z,\theta,\psi) = K_{\mathrm{T}}(z)K_{\mathrm{T}}(\psi)\mathrm{d}\,z[t(\theta)]^{m_{\mathrm{T}}} \tag{10a}$$

$$\mathrm{d}\,F_{\mathrm{R}}(z,\theta,\psi) = K_{\mathrm{R}}(z)K_{\mathrm{R}}(\psi)\mathrm{d}\,z[t(\theta)]^{m_{\mathrm{R}}} \tag{10b}$$

where d $F_{\mathrm{T}}(z, \theta, \psi)$ and d $F_{\mathrm{R}}(z, \theta, \psi)$ are, respectively, the differential tangential and radial cutting force component of a cutting element, which is at a distance z from the cutter tip, at an angular position θ, and at a feed angle ψ with respect to the horizontal plane. The undeformed chip area for the cutting element is represented by the chip width d z and the undeformed chip thickness $t(\theta)$. $K_{\mathrm{T}}(z)$ and $K_{\mathrm{R}}(z)$ are the cutting mechanics parameters for horizontal cutting motions, and $K_{\mathrm{T}}(\psi)$ and $K_{\mathrm{R}}(\psi)$ quantify the effect of ψ on $K_{\mathrm{T}}(z)$ and $K_{\mathrm{R}}(z)$. m_{T} and m_{R} explicitly characterize the size effect in metal cutting.

5.1 Calibration approach

The empirical cutting force coefficients in Eqs. (10a) and (10b) need to be calibrated for each cutter–workpiece material pair in order to calculate the ball-end milling forces. Various approaches for calibrating the cutting force coefficients have been proposed in the literature, such as: processing the instantaneous cutting forces rather than the average cutting forces [36], analyzing the experimental force data in the frequency domain [37], separating the cutting forces into nominal and perturbation components [38], using force data generated from a finite element model [39], and considering the negative effect of cutter runout [40].

Cutting force coefficients obtained from horizontal calibration cuts have been used to calculate cutting forces of a ball-end mill with non-horizontal cutting motions by many researchers. However, the cutting mechanics parameters obtained from horizontal calibration cuts cannot accurately characterize the non-horizontal cutting mechanics. Both the undeformed chip geometry and the chip flow direction in a non-horizontal cut are different from those in a horizontal cut, which would have much impact on the resulting cutting mechanics parameters. Hence, non-horizontal calibration

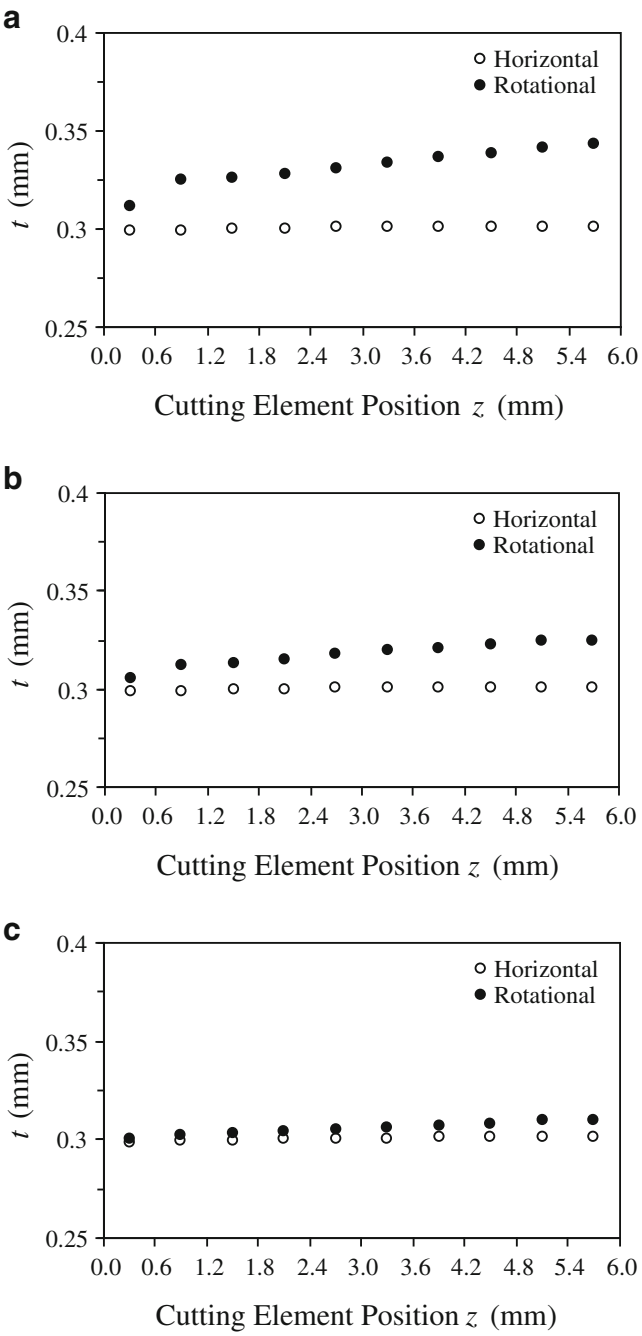

Fig. 7 Undeformed chip thickness values at θ=60° for rotational and horizontal cutting motions: **a** R=90 mm, **b** R=900 mm, and **c** R=9,000 mm (feed at cutter tip 0.337 mm/tooth, axial depth of cut 6 mm, side step 6 mm)

cuts over a desired feed angle range are needed in addition to horizontal calibration cuts. In order to keep the entire calibration procedure simple and efficient, a work part of a specific geometry has been proposed in the present work such that a continuous half-slot cut around the part edges can cover the intended feed angle range. As can been seen in Fig. 8, the proposed work part contains four different

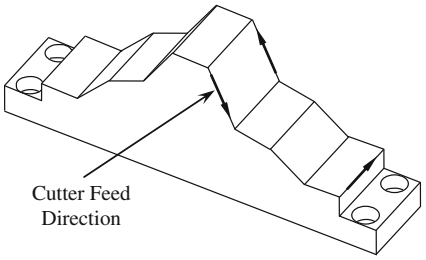

Fig. 8 Work part geometry for the efficient calibration of cutting force coefficients

upward and downward feed-angle faces with an increment of 10° with respect to the horizontal face, i.e., ±10° to ±40°.

5.2 Experimental setup

The continuous half-slot calibration cut was performed on a Wahli-51 five-axis CNC horizontal machining center using an Ingersoll 12-mm TiAlN-coated carbide ball-end mill with a helix angle of 30°. The ball-end mill was held by the collet of the tool holder, which was an integral part of the Kistler 9124A rotating cutting force dynamometer (Fig. 9a). The ensemble unit of the dynamometer, tool holder, and ball-end mill was inserted into the machine spindle to carry out the

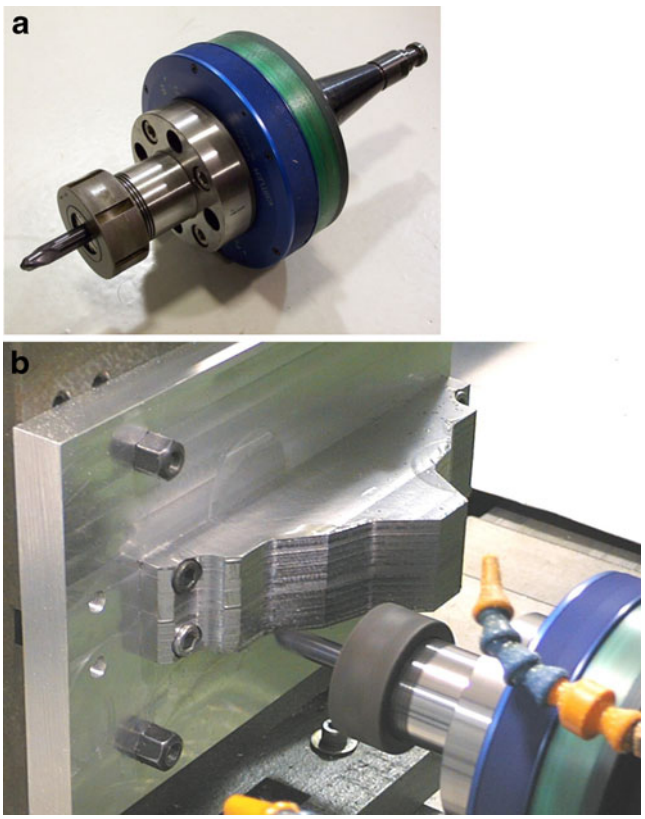

Fig. 9 Machining setup: **a** ensemble unit of dynamometer, tool holder, and ball-end mill and **b** close-up view of ball-end mill and calibration work part

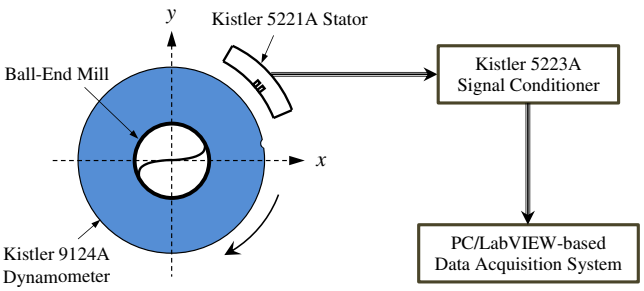

Fig. 10 Overall cutting force measurement setup

ball-end milling experiments and measure the cutting forces. The calibration work part, made of SAE 1018 cold rolled steel, was securely fastened to the rotary machine table. A close-up view of the ball-end mill and the calibration work part is shown in Fig. 9b.

Machining was done without coolant, as recommended by the tool manufacturer. A spindle speed of 948 rpm and a feed rate of 101.6 mm/min (0.054 mm/tooth) were chosen for the calibration cut. The Kistler 9124A rotating cutting force dynamometer was used to measure the instantaneous cutting forces in the cutter lateral (x and y) directions. The measured voltage data were first transmitted to a Kistler 5221A stator, which was mounted on the spindle housing, through a wireless connection. The measurement data were then passed through a Kistler 5223A signal conditioner and into a PC/LabVIEW-based data acquisition system. The data acquisition system was devised to capture and store the digitized cutting force data at a sampling rate of 23.7 kHz, corresponding to 1,500 data points per cutter rotation cycle. The overall cutting force measurement setup is depicted in Fig. 10.

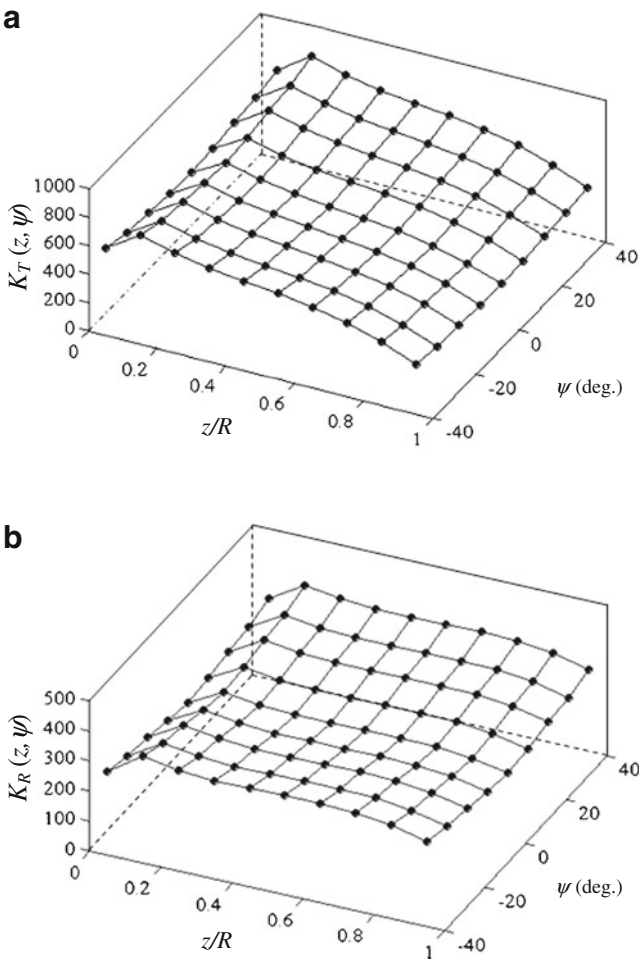

Fig. 11 Variation of the cutting mechanics parameters: **a** $K_T(z, \psi)$ and **b** $K_R(z, \psi)$

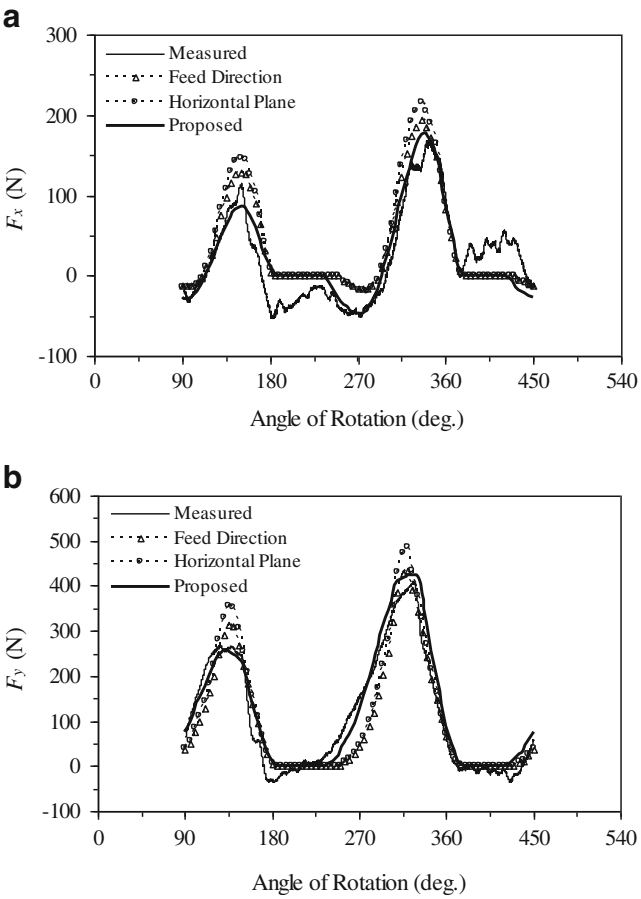

Fig. 12 **a**, **b** Predicted and measured cutting forces for the 20° upward cutting motion (feed 0.054 mm/tooth, axial depth of cut 6 mm, side step 3 mm)

5.3 Calibration results

The cutting force coefficients of $K_T(z)$ and $K_R(z)$ (cutting mechanics parameters for the horizontal cut) and m_T and m_R (size effect parameters) were first determined using the measured instantaneous cutting forces from the horizontal calibration cut [36]. These parameters are then employed to determine $K_T(\psi)$ and $K_R(\psi)$ to characterize the effect of

non-horizontal feed angles. The resulting variation of the combined cutting mechanics parameters $K_T(z, \psi)$ and $K_R(z, \psi)$ along the cutting edge and for the intended feed angle range (±10° to ±40°) is shown in Fig. 11.

6 Experimental validation and discussion

The presented mechanistic cutting force model has been validated experimentally by comparing the predicted cutting forces with the measured ones. The measured cutting forces were obtained from a set of non-transient horizontal, non-horizontal, and rotational test cuts using the same ball-end mill, work material, and experimental setup as those for the calibration cut. By varying the feed rate and radial depth of cut, a total of 33 verification cuts were performed, covering all the three basic cutting motions. In particular, non-horizontal feed angles ranging from ±10° to ±40° (at 10° interval) as well as two cutter tip rotational radii (R=90 and 115 mm) for the rotational cutting motion were employed and tested.

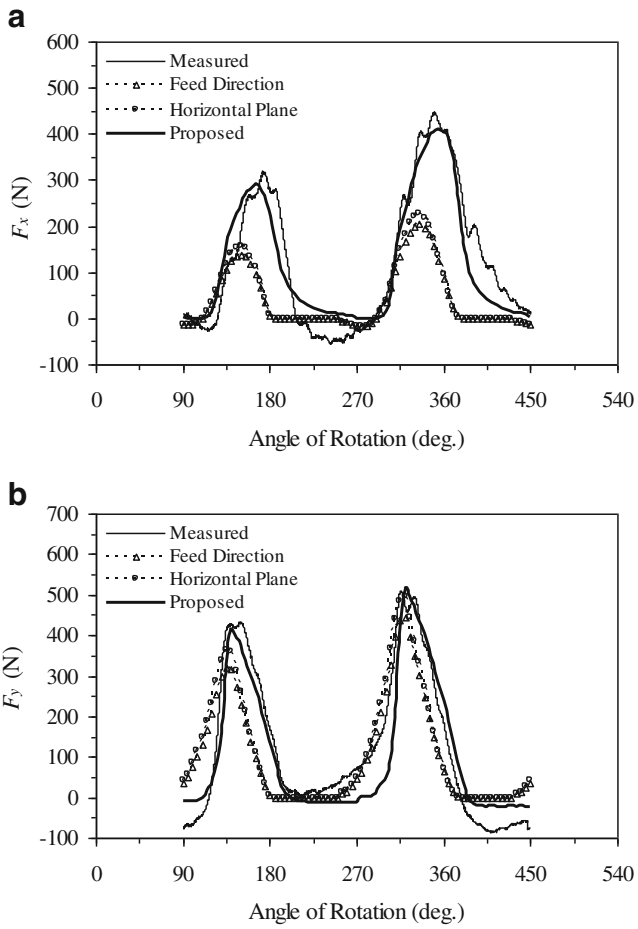

Fig. 13 **a**, **b** Predicted and measured cutting forces for the 20° downward cutting motion (feed 0.054 mm/tooth, axial depth of cut 6 mm, side step 3 mm)

6.1 Non-horizontal cuts

As illustrated in "Section 4", the proposed concept to determine the undeformed chip thickness can lead to significantly different values than those determined by the existing concepts for non-horizontal and rotational ball-end milling cuts. For non-horizontal cuts, the predicted cutting forces for two typical cases (test cut no. 10 with 20° upward cutting motion and test cut no. 13 with 20° downward cutting motion) based on the various undeformed chip thickness determination concepts are compared against the measured cutting forces. The comparison results are shown in Figs. 12 and 13, respectively. It can be seen that the proposed model in this work produced the best match with the measured cutting forces. For the upward cutting motion, models based on the existing undeformed chip thickness determination concepts over-estimate the cutting forces, whereas for the downward cutting motion underestimated cutting forces are observed. The primary reason for the overestimated and underestimated cutting forces by the existing models for non-horizontal cuts is discussed in the following section.

For horizontal cutting motions of a ball-end mill, an engaged cutting element on the cutter and its corresponding cutting elements on the machined surfaces in the previous

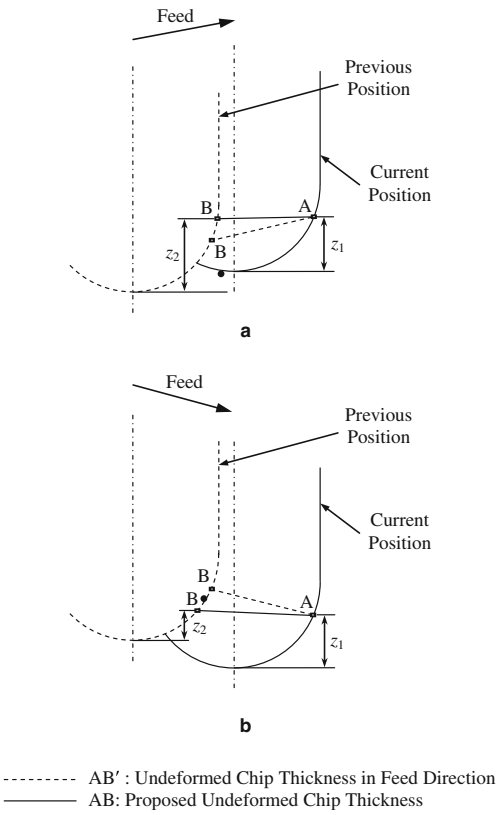

Fig. 14 Overestimation and underestimation of undeformed chip thickness values for an existing concept: **a** upward and **b** downward ball-end milling

Table 1 RMS percentage deviations for non-horizontal cutting motions

Test no.	Cutting force	Proposed	Feed direction		Horizontal plane	
		RMS % deviation	RMS % deviation	Improvement	RMS % deviation	Improvement (%)
10	F_x	7.83	13.11	40.3	11.06	29.2
	F_y	2.49	3.84	35.2	3.60	30.8
13	F_x	3.33	9.41	64.6	9.73	65.9
	F_y	4.76	6.81	30.2	7.11	33.1

cutter rotation cycle all have the same z position with respect to the cutter tip. However, for non-horizontal cutting motions, this is not the case anymore. Depending on the feed angle, the corresponding cutting element on a previously machined surface can be at a higher or lower z position from the cutter tip than the current cutting element. More specifically, for the upward ball-end milling case depicted in Fig. 14a, cutting element A represents the current cutting element, and cutting elements B and B′, respectively, represent the corresponding cutting element on a previously machined surface for the proposed undeformed chip thickness determination concept and the existing concept based on the feed direction. Cutting elements A and B′ are at the same distance z_1 from the cutter tip due to the linear rigid-body motion of the cutter. However, cutting element B, which is determined according to the instantaneous revolving center of A, is at a distance z_2 from the cutter tip, and $z_2 > z_1$. It is then clear that the undeformed chip thickness AB′ determined by the existing concept would be larger than the undeformed chip thickness AB determined by the proposed concept. As a result, the existing concept overestimates the cutting forces as shown in Fig. 12. Similarly for the downward ball-end milling case depicted in Fig. 14b, the undeformed chip thickness AB′ is smaller than AB as $z_2 < z_1$; hence, the existing concept underestimates the actual cutting forces as shown in Fig. 13. A quantified comparison of all the predicted cutting forces in Figs. 12 and 13 is summarized in Table 1 using the root mean square (RMS) of percentage deviations with respect to the measured cutting forces. The comparison results clearly demonstrate the superiority (29.2–65.9 % improvement) of the presented cutting force model over the existing models for non-horizontal cutting motions.

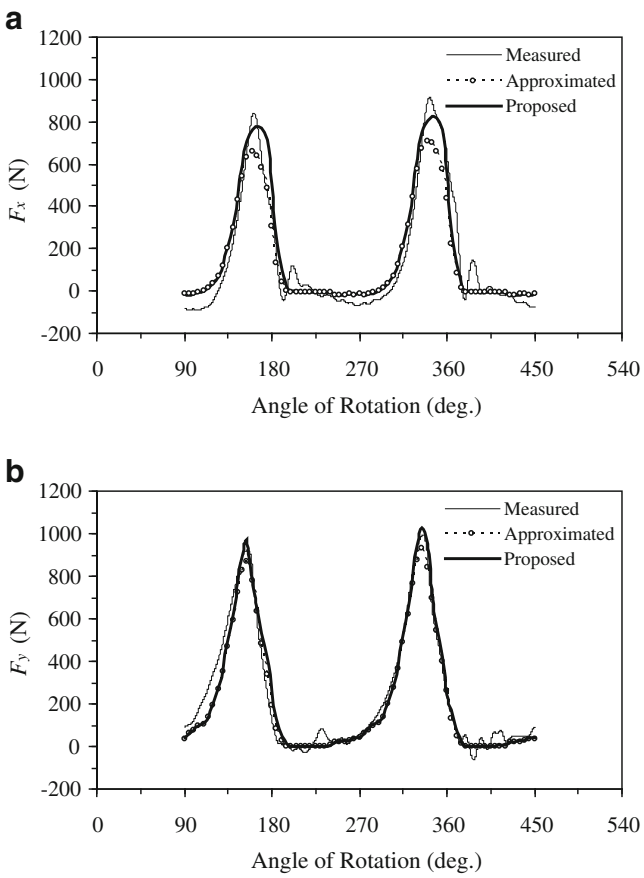

Fig. 15 **a**, **b** Predicted and measured cutting forces for the rotational cutting motion (R=90 mm, feed at cutter tip 0.337 mm/tooth, axial depth of cut 6 mm, side step 3 mm)

6.2 Rotational cuts

For the rotational cutting motion, Fig. 15 compares the predicted cutting forces for a typical case (test cut no. 28 with cutter tip rotational radius R=90 mm) based on two different undeformed chip thickness determination concepts against the measured cutting forces. Unlike horizontal and non-horizontal cutting motions, the verification cuts for rotational cutting motions were performed at a higher feed rate in order to clearly illustrate the advantages of the proposed model. As shown in Fig. 15, the predicted cutting

Table 2 RMS percentage deviations for a rotational cutting motion

Test no.	Cutting force	Proposed	Approximated horizontal	
		RMS % deviation	RMS % deviation	Improvement (%)
28	F_x	3.82	4.85	21.1
	F_y	1.69	1.94	17.7

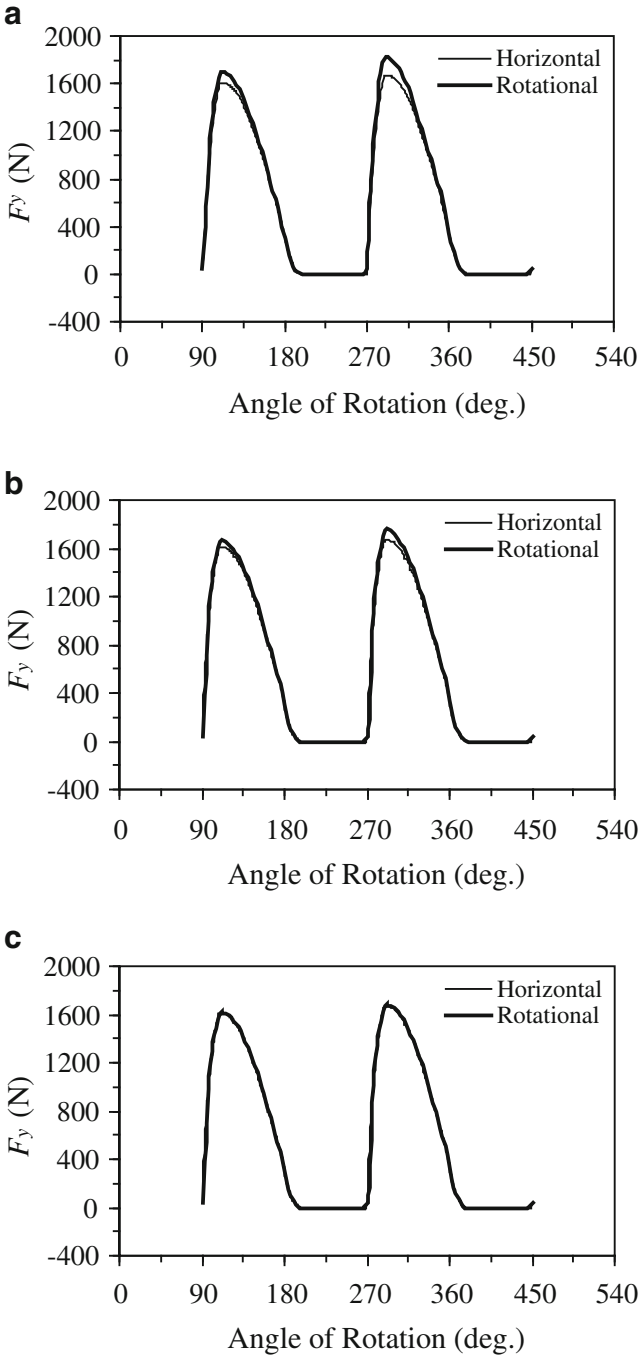

Fig. 16 Predicted cutting forces for rotational and horizontal cuts: **a** R=50 mm, **b** R=100 mm, and **c** R=500 mm (feed at cutter tip 0.337 mm/tooth, axial depth of cut 6 mm, side step 6 mm)

forces from the proposed model show a better agreement with the measured cutting forces than those from a model based on the approximated horizontal concept (described in "Section 4.3") for undeformed chip thickness determination. It is noted in the figure that the approximated horizontal concept results in the underestimation of the actual cutting forces. The reason for the cutting force underestimation is evident, which is due to the underestimated undeformed chip thicknesses using the approximated horizontal concept, as already illustrated in Fig. 6. Table 2 shows the RMS percentage deviations of the predicted cutting forces. Quantified improvements (21.1 % for F_x and 17.7 % for F_y) of the proposed model are observed.

Using the proposed model, the predicted cutting forces for rotational cutting motions with different cutter tip rotational radii are also compared with those for the horizontal cutting motion. Figure 16 shows that the shape of the cutting force profile from a rotational cut is quite similar to that from the horizontal cut. This similarity can be attributed to almost the same cutter–work engagement area on the ball-end mill for the rotational and horizontal cuts. Figure 16 also shows that for relatively small cutter tip rotational radii, the difference between the cutting forces for the rotational and horizontal cuts is fairly significant. However, with increasing cutter tip rotational radius, the cutting forces for the rotational cut approach those for the horizontal cut. It is then clear that only for a very large cutter tip rotational radius (very high R/r ratio) can a rotational cut be reliably approximated as a horizontal cut.

7 Conclusions

In multi-axis ball-end milling, horizontal, non-horizontal, and rotational cutting motions of the cutter are common. This paper has presented an improved mechanistic model that can reliably predict the cutting forces for all of these three basic cutting motions of a ball-end mill. The main contributions of this paper are:

- A generalized concept for undeformed chip thickness determination based on the 3D cutting element trajectories for the particular cutting motion
- A specific work part design to simplify the calibration procedure of the involved cutting force coefficients

The horizontal, non-horizontal, and rotational cutting motions of a ball-end mill are individually considered in this work, yet the presented undeformed chip thickness determination concept is generic and readily applicable to any combination of these basic cutting motions. It can be applied to other milling cutters in the same way. It should be pointed out that reliable cutting force predictions, in particular for multi-axis complex sculptured surface machining, require accurate identification of the instantaneous cutter–work engagement area on the ball-end mill. Such research is being pursued by researchers in order to develop a virtual machining system to reliably simulate the cutting mechanics and dynamics in the multi-axis machining of sculptured surfaces.

Acknowledgments This research was in part funded by the Natural Sciences and Engineering Research Council of Canada and Materials and Manufacturing Ontario. The bulk of this work was completed when the authors were with the Department of Mechanical and Materials Engineering at the University of Western Ontario. The authors wish to thank Dave Kingston and Marcel Verner of the former Integrated Manufacturing Technologies Institute, National Research Council of Canada, for their technical assistance in conducting the experiments. Ingersoll Cutting Tool Company is also gratefully acknowledged for providing the ball-end mills for the experimental work.

References

1. Martellotti ME (1941) An analysis of the milling process. Trans Am Soc Mech Eng 63:677–700
2. Kline WA, DeVor RE, Lindberg JR (1982) The prediction of cutting forces in end milling with application to cornering cuts. Int J Mach Tool Des Res 22:7–22
3. Kline WA, DeVor RE (1983) The effect of runout on cutting geometry and forces in end milling. Int J Mach Tool Des Res 23:123–140
4. Sutherland JW, DeVor RE (1986) An improved method for cutting force and surface error prediction in flexible end milling systems. ASME J Eng Ind 108:269–279
5. Li HZ, Liu K, Li XP (2001) A new method for determining the undeformed chip thickness in milling. J Mater Process Technol 113:378–384
6. Kumanchik LM, Schmitz TL (2007) Improved analytical chip thickness model for milling. Precis Eng 31:317–324
7. Sai L, Bouzid W, Zghal (2008) A chip thickness analysis for different tool motions for adaptive feed rate. J Mater Process Technol 204:213–220
8. Yucesan G, Altintas Y (1994) Improved modeling of cutting force coefficients in peripheral milling. Int J Mach Tool Manuf 34:473–487
9. Budak E, Altintas Y, Armarego EJA (1996) Prediction of milling force coefficients from orthogonal cutting data. ASME J Manuf Sci Eng 118:216–224
10. Yang M, Park H (1991) The prediction of cutting force in ball-end milling. Int J Mach Tool Manuf 31:45–54
11. Yucesan G, Altintas Y (1996) Prediction of ball-end milling forces. ASME J Eng Ind 118:95–103
12. Zhu R, Kapoor SG, DeVor RE (2001) Mechanistic modeling of the ball end milling process for multi-axis machining of free-form surfaces. ASME J Manuf Sci Eng 123:369–379
13. Fussell BK, Jerard RB, Hemmett JG (2003) Modeling of cutting geometry and forces for 5-axis sculptured surface machining. Comput Aided Des 35:333–346
14. Milfelner M, Cus F (2003) Simulation of cutting forces in ball-end milling. Robot Comput Integr Manuf 19:99–106
15. Gradisek J, Kalveram M, Weinert K (2004) Mechanistic identification of specific force coefficients for a general end mill. Int J Mach Tool Manuf 44:401–414
16. Feng HY, Menq CH (1994) The prediction of cutting forces in the ball-end milling process—I. Model formulation and model building procedure. Int J Mach Tool Manuf 34:697–710
17. Jung YH, Kim JS, Hwang SM (2001) Chip load prediction in ball-end milling. J Mater Process Technol 111:250–255
18. Lazoglu I (2003) Sculpture surface machining: a generalized model of ball-end milling force system. Int J Mach Tool Manuf 43:453–462
19. Ko JH, Cho DW (2005) 3D ball-end milling force model using instantaneous cutting force coefficients. ASME J Manuf Sci Eng 127:1–12
20. El-Mounayri H, Briceno JF, Gadallah M (2010) A new artificial neural network approach to modeling ball-end milling. Int J Adv Manuf Technol 47:527–534
21. Lopez de Lacalle LN, Lamikiz A, Sanchez JA, Salgado MA (2007) Toolpath selection based on the minimum deflection cutting forces in the programming of complex surfaces milling. Int J Mach Tool Manuf 47:388–400
22. Tsai CL, Liao YS (2010) Cutting force prediction in ball-end milling with inclined feed by means of geometrical analysis. Int J Adv Manuf Technol 46:529–541
23. Cao Q, Xue D, Zhao J, Li Y (2011) A cutting force model considering influence of radius of curvature for sculptured surface machining. Int J Adv Manuf Technol 54:821–835
24. Melkote SN, Endres WJ (1998) The importance of including size effect when modeling slot milling. ASME J Manuf Sci Eng 120:68–75
25. Lamikiz A, Lopez de Lacalle LN, Sanchez JA, Salgado MA (2004) Cutting force estimation in sculptured surface milling. Int J Mach Tool Manuf 44:1511–1526
26. Fontaine M, Devillez A, Moufki A, Dudzinski D (2006) Predictive force model for ball-end milling and experimental validation with a wavelike form machining test. Int J Mach Tool Manuf 46:367–380
27. Fontaine M, Moufki A, Devillez A, Dudzinski D (2007) Modelling of cutting forces in ball-end milling with tool–surface inclination. Part I: predictive force model and experimental validation. J Mater Process Technol 189:73–84
28. Fontaine M, Devillez A, Moufki A, Dudzinski D (2007) Modelling of cutting forces in ball-end milling with tool–surface inclination. Part II: influence of cutting conditions, run-out, ploughing and inclination angle. J Mater Process Technol 189:85–96
29. Feng HY, Menq CH (1996) A flexible ball-end milling system model for cutting force and machining error prediction. ASME J Manuf Sci Eng 118:461–469
30. Ikua BW, Tanaka H, Obata F, Sakamoto S (2001) Prediction of cutting forces and machining error in ball end milling of curved surfaces—I. Theoretical analysis. Precis Eng 25:266–273
31. Sun Y, Ren F, Guo D, Jia Z (2009) Estimation and experimental validation of cutting forces in ball-end milling of sculptured surfaces. Int J Mach Tool Manuf 49:1238–1244
32. Kim GM, Cho PJ, Chu CN (2000) Cutting force prediction of sculptured surface ball-end milling using Z-map. Int J Mach Tool Manuf 40:277–291
33. Ozturk E, Tunc LT, Budak E (2009) Investigation of lead and tilt angle effects in 5-axis ball-end milling processes. Int J Mach Tool Manuf 49:1053–1062
34. Ozturk E, Budak E (2010) Dynamics and stability of five-axis ball-end milling. ASME J Manuf Sci Eng 132(021003):1–13
35. Feng HY, Su N (2001) A mechanistic cutting force model for 3D ball-end milling. ASME J Manuf Sci Eng 123:23–29
36. Azeem A, Feng HY, Wang L (2004) Simplified and efficient calibration of a mechanistic cutting force model for ball-end milling. Int J Mach Tool Manuf 44:291–298
37. Zhang Z, Zheng L, Zhang L, Li Z, Liu D, Zhang B (2005) A study on calibration of coefficients in end milling forces model. Int J Adv Manuf Technol 25:652–662
38. Wan M, Zhang WH, Qin GH, Tan G (2007) Efficient calibration of instantaneous cutting force coefficients and runout parameters for general end mills. Int J Mach Tool Manuf 47:1767–1776
39. Gonzalo O, Jauregi H, Uriarte LG, Lopez de Lacalle LN (2009) Prediction of specific force coefficients from a FEM cutting model. Int J Adv Manuf Technol 43:348–356
40. Riviere-Lorphevre E, Filippi E (2009) Mechanistic cutting force model parameters evaluation in milling taking cutter radial runout into account. Int J Adv Manuf Technol 45:8–15